# Carbon Nanotubes: Electronic Structure and Physical Properties

Discovered in 1991, carbon nanotubes are molecules of pure carbon having the shape of a long, hollow cylinder with diameter in the nanometer range. More precisely stated, a nanotube is a cylindrical variety of graphite. A single-wall nanotube is just one atomic layer thick, that is, one seamless rolled-up graphene layer. Multiwall nanotubes are composed of several coaxial graphitic layers, with a separation distance of 0.34 nm. The electronic properties of a thick multiwall nanotube resemble those of graphite, which is semimetallic. Remarkably enough, a single-wall nanotube can be a metal or a semiconductor depending on its exact atomic structure. A metallic single-wall nanotube often conducts electrons ballistically, which means that electrons flow through it over long distances (micrometers) without collisions. A semiconducting single-wall nanotube has a bandgap 0.6 eV, depending on its diameter.

Many physical properties of a nanotube depend on its remarkable electronic structure. Transport properties and optical properties of the nanotubes are, of course, directly linked to its electronic band structure. The response of a nanotube to an external field also depends on its electronic structure: transistor effect and field emission are two important phenomena taking place upon application of an electric field. All these aspects are discussed below.

## 1. *Electronic Structure*

### *1.1 π-Electron Zone-folding Approximation*

Conceptually, a single-wall nanotube can be constructed by rolling up a graphene strip of arbitrary length into a seamless cylinder. The basic construction is shown in Fig. 1(a) where the universally used wrapping indices $(n, m)$ are defined. The rolling-up operation brings the $(n, m)$ node of the graphene sheet onto the origin $O$.

The starting point for understanding the electronic properties of a nanotube is the band structure of graphene. Close to the Fermi energy, the band structure of graphene is dominated by the $\pi$ states formed by the interacting $2p_z$ orbitals normal to the atomic plane. Since graphene contains two atoms in its unit cell, there are two $\pi$ bands, a bonding ($\pi$) one and an antibonding ($\pi^*$) one. In the linear combination of atomic orbital (LCAO) approximation (Wallace 1947), the dispersion of these two bands in the two-dimensional reciprocal space of the wave vector $\mathbf{k}$ follows a simple analytical expression

$$E_{\pm}(\mathbf{k}) = \varepsilon_\pi \pm \frac{\gamma_0 |F(\mathbf{k})|}{1 \mp S|F(\mathbf{k})|} \qquad (1)$$

where $\gamma_0 = |V - S\varepsilon_\pi|$, $S$ and $V$ being the overlap and hopping integrals between two nearest-neighbor $2p_z$ orbitals, respectively, and $\varepsilon_\pi$ is the energy of these orbitals. The upper sign in Eqn. (1) is for the unoccupied

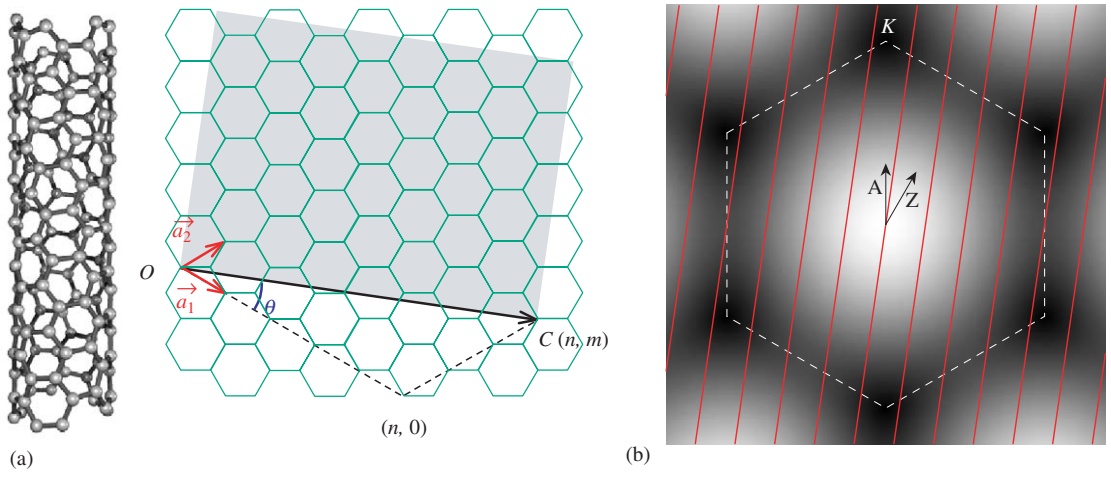


***Figure 1***
(a) Graphene sheet representing a planar development (shaded area) of the nanotube $(n, m)$ for $n = 5$ and $m = 3$. $\theta$ is the chiral angle. In the rolled-up structure, $OC$ is the circumference of the nanotube. (b) Gray-scale map of the separation between the $\pi^*$ and $\pi$ bands of graphene (black corresponds to 0, white to 6.9 eV) in the reciprocal plane of graphene. The $\Gamma$ point is at the center of the figure. The boundaries of the first Brillouin zone are shown by the dashed lines. The thick lines across the drawing are discretization lines of the Bloch vector for the (5, 3) nanotube, parallel to its axis. The two arrows indicate the axial direction of armchair (A) ($m = n$) and zigzag (Z) ($m = 0$) nanotubes.

$\pi^*$ band, the lower sign is for the occupied $\pi$ band, $F(\mathbf{k}) = 1 + \exp(i\mathbf{k}\cdot\mathbf{a}_1) + \exp(i\mathbf{k}\cdot\mathbf{a}_2)$ with $\mathbf{a}_1$ and $\mathbf{a}_2$ being two primitive translation vectors of the graphene hexagonal lattice. The best values of the parameters in Eqn. (1) are $\gamma_0 = 2.9\,\text{eV}$, $S = 0.13$.

The separation between the $\pi^*$ and $\pi$ bands in the reciprocal plane of graphene is represented in Fig. 1(b). These bands cross each other at the corners of the hexagonal first Brillouin zone, the $K$ points, where the function $F(\mathbf{k})$ vanishes. For symmetry reasons, the Fermi level coincides with the energy $\varepsilon_\pi$ of the band crossing. Graphene is a zero-gap semiconductor; its density of states at the Fermi energy $E_F$ is zero and increases linearly on both sides of $E_F$.

In a single-wall nanotube, cyclic boundary conditions apply around the circumference. In the planar presentation shown in Fig. 1(a), the circumference of the nanotube is a translation vector of graphene, $\mathbf{C} = n\mathbf{a}_1 + m\mathbf{a}_2$ with $n$ and $m$ being the wrapping indices. In the two-dimensional graphene sheet, the wave function at the endpoint of $\mathbf{C}$ is the one at the origin multiplied by the Bloch factor $\exp(i\mathbf{k}\cdot\mathbf{C})$. Assuming that the graphene wave functions remain valid in the rolled-up structure (zone-folding approximation), these cyclic boundary conditions impose $\exp(i\mathbf{k}\cdot\mathbf{C}) = 1$. This condition discretizes the Bloch vector $\mathbf{k}$ along equidistant lines $\mathbf{k}\cdot\mathbf{C} = 2\pi\ell$ perpendicular to $\mathbf{C}$ and therefore parallel to the nanotube axis, where $\ell$ is an integer number. These discretization lines are drawn in Fig. 1(b). Along each of these lines, the $\pi$ and $\pi^*$ bands of graphene are sampled. Both bands are always separated by a gap, unless a discretization line passes exactly through a corner $K$ of the first Brillouin zone. The nanotube is then a metal, because it contains two bands that cross the Fermi level. This happens when $nK_1 + mK_2 = \ell$, where $K_1$ and $K_2$ are the coordinates of a $K$ point in the basis formed by the reciprocal unit vectors of graphene. Taking $K_1 = 1/3$ and $K_2 = -1/3$ leads to the condition $n - m = 3\ell$. In other words, $n - m$ must be a multiple of 3 in order to obtain a metallic nanotube, otherwise the nanotube is a semiconductor (Hamada *et al.* 1992). An armchair nanotube ($n = m$) is always a metal. This can be seen directly from Fig. 1(b): a line drawn along the arrow marked A always intersects the upper $K$ point of the first Brillouin zone.

The bandgap of a semiconducting nanotube is easily calculated. Close to the $K$ point, the function $F(\mathbf{k})$ can be linearized with respect to the distance $\delta\mathbf{k}$ of the wave vector $\mathbf{k}$ from the $K$ point. To first order in $\delta\mathbf{k}$, Eqn. (1) simplifies in

$$E_\pm(\delta\mathbf{k}) = \varepsilon_\pi \pm \tfrac{3}{2}\gamma_0 d_{CC}|\delta\mathbf{k}| \qquad (2)$$

where $d_{CC}$ is the CC bond length (0.14 nm). As can be seen in Fig. 1(b), the closest distance of the discretization lines to a $K$ point for a semiconductor is one-third the separation between these lines, which is the reciprocal of the nanotube radius. Setting $|\delta\mathbf{k}| = 2/3d$, with $d$ the nanotube diameter, in the above equation leads to the smallest possible energy of the $\pi^*$ states and the largest possible value of the $\pi$ states. The separation between them is the bandgap, $E_g = 2\gamma_0 d_{CC}/d$. This formula is asymptotically correct for large $d$.

### 1.2 Electronic Structure

For small diameter ($d < 1.2$ nm), the linear and isotropic dependence of the energy of the $\pi^*$ and $\pi$ bands (Eqn. (2)) is no longer valid even at the distance of closest approach of the discretization lines to the $K$ point. Corrections to the $1/d$ dependence of the bandgap are required, with the leading term being proportional to $-r\cos(3\theta)/d^2$. Here, $\theta$ is the chiral angle represented in Fig. 1(a) and $r = +1$ or $-1$ is such that $n - m = M(3) + r$, where $M(3)$ means an integer multiple of 3. Furthermore, the $\pi$ orbitals, being locally oriented along the normal to the nanotube, are not parallel to each other as in graphene. They mix with the $\sigma$ orbitals of neighboring sites. This mixing, although small, lifts the degeneracy of the $\pi$ and $\pi^*$ states at the $K$ point. A small gap opens for these nanotubes for which $n - m = M(3)$, except for the armchair nanotubes ($n$, $n$) where the crossing of the bands at $\varepsilon_\pi$ is still allowed, due to the $\mathbf{C}_{nv}$ symmetry for all Bloch wave vectors.

More refined electronic theories are required to account for the curvature-induced effects, such as tight-binding models including all the valence electrons of **C** and *ab initio* techniques, generally based on the local-density approximation. We show here below the results of a nonorthogonal tight-binding model that incorporates the $2s$ and $2p$ orbitals of **C** (Popov 2004). The calculated bandgap of all nanotubes with diameter smaller than 2.4 nm is represented by the lowest curve in Figs. 2(a) and 2(b). In Fig. 2(a), one clearly sees the rapid closing ($1/d^2$ law) of the gap upon increasing the diameter of the "pseudo-metallic" nanotubes (those for which $n - m = M(3) \neq 0$). For $d >$ 1.2 nm, the bandgap of the semiconducting nanotubes ($n - m = M(3) \pm 1$) shown by the lowest curve in Fig. 2(b) follows reasonably well the $1/d$ law predicted by the zone-folding approximation. Below that diameter, the bandgap becomes dependent on the chirality of the nanotube, as can be observed in Fig. 2(b).

The electron band structure represented against the one-dimensional wave vector and the density of states of two nanotubes, a metal and a semiconductor, are shown in Figs. 3(a) and 3(b). In the band structure of the metallic nanotube (Fig. 3(a)), two branches derived from the $\pi$ and $\pi^*$ bands of graphene cross at the Fermi level. These branches have a nearly linear dispersion around the Fermi wave vector. According to Eqn. (2), their slope is $\hbar v_F = \pm 3\gamma_0 d_{CC}/2$, where $v_F$ is the Fermi velocity. With the same approximation, the HOMO and LUMO bands of a semiconducting nanotube (Fig. 3(b)) have a hyperbolic dispersion

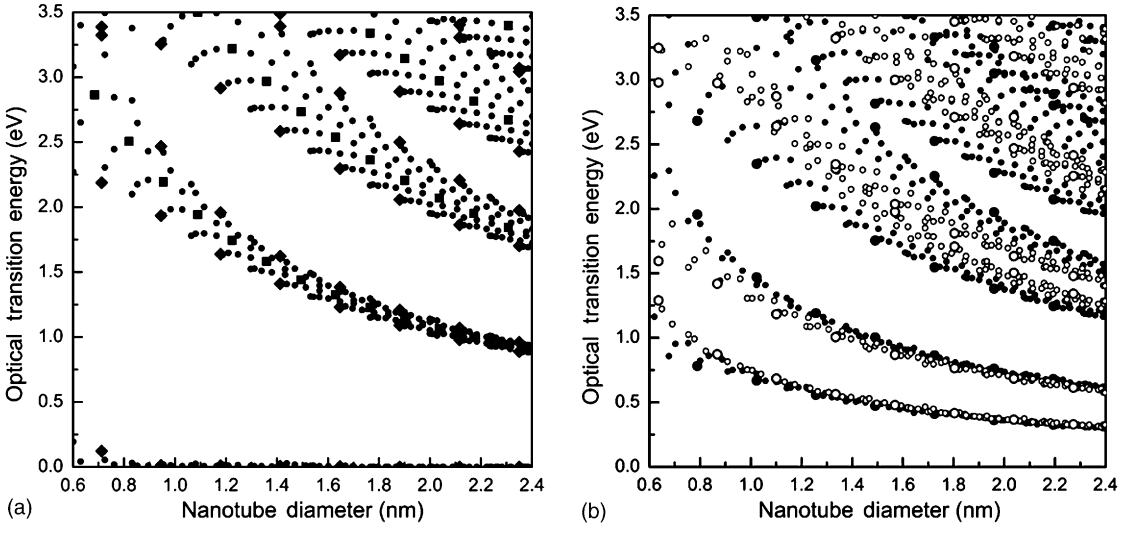


*Figure 2*
Optical transition energies computed with a nonorthogonal tight-binding model for $(n, m)$ nanotubes with (a) $n - m = M(3)$ (metals) and (b) $n - m = M(3) + r$ (semiconductors) vs. diameter. In (a) squares are for armchair nanotubes ($m = n$), diamonds for zigzag tubes ($m = 0$), and circles for chiral nanotubes ($0 < m < n$). In (b), open symbols correspond to $r = -1$ and black symbols correspond to $r = +1$; large circles are for zigzag and small circles for chiral nanotubes.

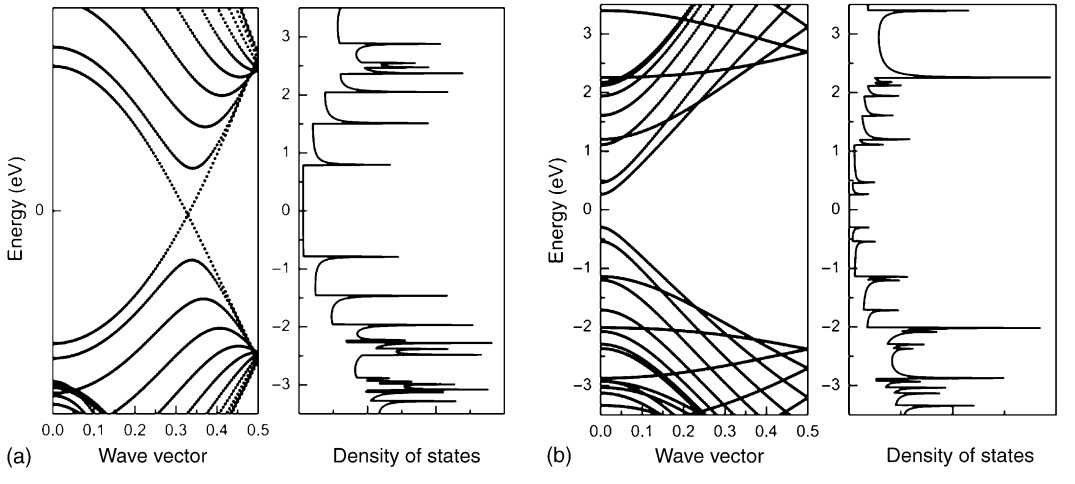


*Figure 3*
Electronic band structure and density of states of (a) the (10,10) armchair nanotube and (b) the (17, 0) zigzag nanotube, computed with a nonorthogonal tight-binding model. The wave vector in the band structures is given in units of $2\pi/a$ with $a$ the translational period of the nanotube.

relation

$$E_{\pm}(\mathbf{k}) = \varepsilon_{\pi} \pm \sqrt{(E_g/2)^2 + (3\gamma_0 d_{CC}/2)^2 (k - k_m)^2} \quad (3)$$

where $k_m$ is the wave vector in the first Brillouin zone of the nanotube where the bandgap is located. A metallic nanotube has a nearly constant density of states around the Fermi level. This plateau is generated by the two bands that cross at the Fermi energy. The density of states of a nanotube is characterized by a series of asymmetric spikes, called van Hove singularities, arising at all energies where a branch

has a horizontal slope in the band structure. These singularities form a real fingerprint of the nanotube. Their positions can be measured by scanning tunneling microscopy (STM) (Wildoer *et al.* 1998).

### *1.3 Multiwall Nanotubes*

Roughly stated, the electronic properties of multiwall nanotubes resemble those of graphite, which is semimetallic, as indicated by valence-band photoemission spectroscopy. These nanotubes present a rich variety of transport properties, briefly discussed in a separate section below. In principle, a multiwall nanotube mixes metallic and semiconducting layers. The presence of small interlayer coupling and the fact that the diameters of the constituent layers are larger than a few nanometers (which means small bandgaps) imply that the distinction between metal and semiconductor is not as pronounced as in single-wall nanotubes. However, both semiconducting and metallic characteristics were found by STM measurements performed on individual multiwall nanotubes. Furthermore, STM spectra may vary strongly from one place to another along the same tube, which may be due to the presence of defects. Defects such as pentagons, heptagons, impurities, and also a bamboo-like structure with the compartmentation of the internal layers, affect the electronic properties of a nanotube. Different parts of it may have different electronic properties (Ebbesen *et al.* 1996).

## *2. Transport Properties*

### *2.1 Landauer Conductance*

The transport properties of a single-wall nanotube (either a metal or a doped semiconductor) deviate significantly from Ohm's law because the charge carriers can flow over a large distance ($\sim 1\,\mu$m at room temperature), without suffering from inelastic scattering by phonons and other excitations. Even in the absence of any scattering of the charge carriers, the resistance of a nanotube is not zero. The reason is that the nanotube offers only a few propagating states in comparison with the macroscopic contact electrodes that have many such states. At small bias, the conductance of the nanotube is indeed controlled by the probability that an electron entering the nanotube from one electrode with Fermi energy $E_F$ can be transmitted to any state with the same energy in the other electrode. The transmitted current is $I = GV$ with $G$ the differential conductance given by

$$G = \frac{2e^2}{h} \sum_n T_n(E_F) \qquad (4)$$

Here the sum is over all nanotube electronic states $n$ at the Fermi energy $E_F$ and that can carry a current in one direction, and $T_n$ is the transmission probability for the conducting state $n$ (also called a channel). Equation (4) is the Landauer–Büttiker formula (Landauer 1970). In the case of a perfect nanotube at zero temperature, $T_n = 1$ for all states, and $G = (2e^2/h)M$ with $M$ the number of branches that cross $E_F$ with a positive $dE/dk$ slope. The electrical resistance is therefore $G^{-1} = h/(2e^2M) = 12.9/M\,\text{k}\Omega$. It is length-independent (ballistic transport) and quantized due to the finite number $M$ of conducting channels. For a metallic nanotube, $M = 2$ when $E_F$ is close to the charge neutrality level $\varepsilon_\pi$. There are indeed two branches with positive slope crossing $\varepsilon_\pi$, one at positive $k$ (shown in Fig. 3(a)), the other at the opposite wave vector $-k$. In practice, the resistance of a metallic nanotube can be significantly larger than $6.45\,\text{k}\Omega$ when there are poor coupling contacts with the external electrodes. In addition, bending, squashing, or twisting a nanotube may affect its conductivity, sometimes inducing a metal–semiconductor transformation.

### *2.2 Effect of Defects*

The scattering of electrons by phonons and defects is expected to increase the electrical resistance. And indeed, the resistance of a nanotube increases slightly with increasing temperature above room temperature, due to the back scattering of electrons by thermally excited phonons (Kane *et al.* 1998). At low temperature, the resistance of an isolated metallic nanotube also increases upon cooling. This unconventional behavior for a metallic system may be the signature of electron correlation effects, first observed in bundles of single-wall nanotubes (Luttinger liquid, typical of one-dimensional systems) (Bockrath *et al.* 1999). A single impurity, such as B or N, in a metallic nanotube affects only weakly the conductivity close to $\varepsilon_\pi$. The same holds true with a Stone–Wales defect, which transforms four adjacent hexagons in two pentagons and two heptagons. Interestingly, even long-range disorder induced by defects such as substitutional impurities has a vanishing back-scattering cross section in metallic nanotubes, at least when $E_F$ is close to $\varepsilon_\pi$. This is not true with doped semiconducting nanotubes, where scattering by long-range disorder is effective.

### *2.3 Multiwall Nanotubes*

The transport regime in multiwall nanotubes is not as well established as for single-walled nanotubes. Experiment shows that they have a wide spectrum of transport properties. Some multiwall nanotubes are metallic or semimetallic, others are clearly nonmetallic. It is generally admitted that electron transport in a metallic multiwall nanotube at room temperature is not ballistic but instead, diffusive (Bachtold *et al.*

2000). However, evidences also exist for ballistic transport taking place in the outermost shell of an individual nanotube in contact with a liquid metal (Frank *et al*. 1998).

The room-temperature resistivity of annealed, large multiwall nanotubes is $2 \times 10^{-6}\,\Omega$m and their resistance per unit length is typically $30\,\mathrm{k}\Omega\,\mu\mathrm{m}^{-1}$. They can carry a very large current density without failure, $10^{11}\,\mathrm{A\,m}^{-2}$. By decreasing temperature below room value, the resistance of an individual nanotube generally increases slightly. At low temperature, this unconventional behavior is often interpreted as being the result of an increase of the elastic back-scattering cross section of the electrons by defects, due to quantum interferences. This happens when the phase coherence length of the electrons, which increases upon cooling, becomes larger than the length of the nanotube.

## 3. Other Properties

### 3.1 Optical Properties

The optical properties of single-wall carbon nanotubes are mainly determined by electronic transitions between van Hove singularities where there is a large accumulation of states in their density of states. For light polarized parallel to the nanotube axis, transitions between symmetric states with respect to the charge neutrality level $\varepsilon_\pi$ are allowed. Among these, the transition across the direct bandgap of the semiconducting nanotubes has the lowest energy. It corresponds to a first optical absorption band at about $E_{11}^{\mathrm{s}} = E_{\mathrm{g}} \sim 0.6\,\mathrm{eV}$ for usual nanotubes (those with diameter $\sim 1.4\,\mathrm{nm}$). The simple zone-folding approximation predicts another absorption band at about twice this energy $E_{22}^{\mathrm{S}}$, still for the semiconducting nanotubes (see Table 1). As for the metallic single-wall nanotubes, the transition between the van Hove singularities located on both sides of the metallic plateau of their density of states (see Fig. 3(a)) has an energy $E_{11}^{\mathrm{M}}$ given in Table 1, which is typically 1.8 eV.Calculated optical transitions between 0.0 eV and 3.5 eV are represented in Figs. 2(a) and 2(b) for all single-wall nanotubes with diameter between 0.6 nm and 2.4 nm.The branch ending at 1 eV for $d = 2.4\,\mathrm{nm}$ in Fig. 2(a) represents the variations of $E_{11}^{\mathrm{M}}$

***Table 1***
First optical transition energies in semiconducting and metallic nanotubes predicted by the π-electron zone-folding approximation (correct to first order in $1/d$, where $d$ is the nanotube diameter).

| Semiconductor | Metal |
|---|---|
| $E_{11}^{\mathrm{S}} = 2\gamma_0 d_{\mathrm{CC}}/d$ | |
| $E_{22}^{\mathrm{S}} = 4\gamma_0 d_{\mathrm{CC}}/d$ | $E_{11}^{\mathrm{M}} = 6\gamma_0 d_{\mathrm{CC}}/d$ |
| $E_{33}^{\mathrm{S}} = 8\gamma_0 d_{\mathrm{CC}}/d$ | |

for metallic nanotubes. The lowest two curves in Fig. 2(b) correspond to $E_{11}^{\mathrm{S}}$ and $E_{22}^{\mathrm{S}}$ in semiconductors. There is some spread of data points compared to the simple $1/d$ laws given in Table 1, which increases with decreasing diameter. The zigzag nanotubes deviate most from these simple laws.

Spectrofluorimetry allows one to probe both first and second transition energies in semiconducting nanotubes. In this type of experiment, a nanotube is excited with a radiation of energy $E_{22}^{\mathrm{S}}$ and it reemits light of energy $E_{11}^{\mathrm{S}}$. Provided the nanotubes are isolated from each other by surfactants in a solution, wrapping indices can be assigned to each measured pair of optical transition energies. The transition energies determined in this way are larger than the predictions of the nonorthogonal tight-binding model by 0.3 eV (Popov 2004). For not too small diameters, the correction to the band-structure model is attributed to self-energy and excitonic effects.

Resonant Raman spectroscopy is another widely used characterization technique that can explore the optical properties of nanotubes. The Raman cross section is considerably increased when either the excitation light or the Raman scattered radiation matches an optical transition energy (Rao *et al*. 1997). These are the conditions for having a resonant Raman scattering. For single-wall nanotubes, the radial breathing mode, that is, a Raman active vibration with uniform radial atomic displacements, is extremely useful for the characterization. This is because the angular frequency of this mode depends on the tube diameter, $\omega_{\mathrm{RBM}} = A/d$, with $A \sim 248\,\mathrm{cm}^{-1}\,\mathrm{nm}$. By measuring $\omega_{\mathrm{RBM}}$ versus laser energy for those nanotubes which are in resonance, two structural informations are obtained: the diameter (via $\omega_{\mathrm{RBM}}$) and the electronic transition energy (from the resonance condition), from which an ($n$, $m$) assignment can be performed (Fantini *et al*. 2004). In resonant Raman spectroscopy of an individual nanotube, it is possible to identify the tube as being metallic or semiconducting from the shape of the tangential Raman band, located near $1580\,\mathrm{cm}^{-1}$, which is asymmetric in a metallic tube due to the coupling of this phonon band with plasmons.

### 3.2 Transistor Effect

The most spectacular potential application of semiconducting single-wall nanotubes in nanoelectronics is their use as a three-terminal device that works like a field effect transistor (FET) (Martel *et al*. 1998, Tans *et al*. 1998). In this application, a nanotube is attached to two metallic electrode lines, acting, respectively, as a source and a drain. The nanotube is separated from a third electrode, the gate, by a thin insulating layer (see Fig. 4(a)). Due to the difference of work function between the nanotube and the electrodes, Schottky barriers are usually formed at the interfaces with the contacts. The valence and

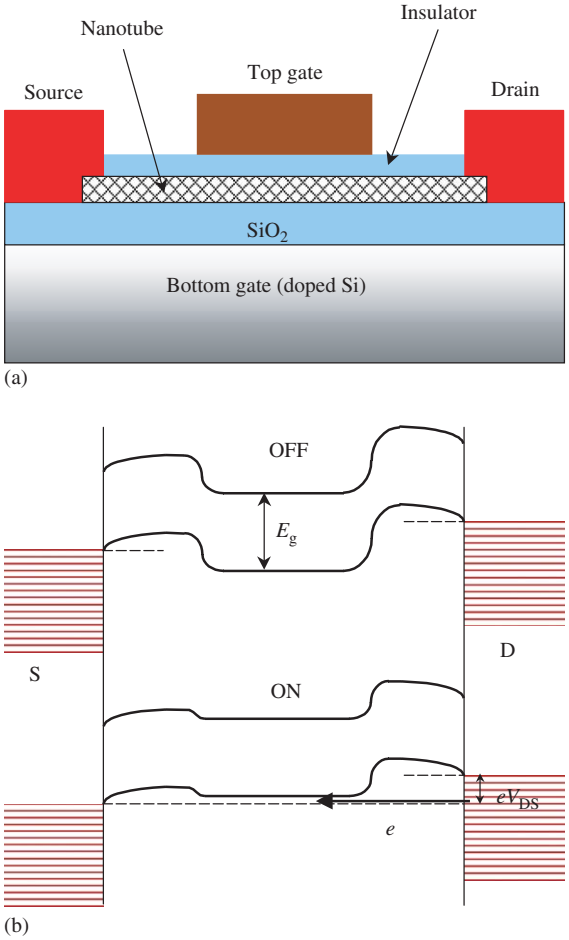


***Figure 4***
(a) Schematic representation of a nanotube FET with its three metallic electrodes (source, drain, and top gate). (b) Simplified band diagram showing the functioning of the FET supposed to be *p*-doped by field effect from the bottom gate. The source (S) and drain (D) electrodes are supposed to have a work function close to that of the semiconducting nanotube. A small positive potential $V_{DS}$ is applied to the drain to bias the nanotube. The top gate has a smaller work function than the nanotube. When the top gate is at a zero or slightly negative potential $V_{GS}$, the transistor is in an OFF state due to the band bending. A negative $V_{GS}$ potential moves the HOMO and LUMO bands of the nanotube upwards. In the ON state, electrons can flow from the drain to the source as indicated by the arrow marked with *e*.

conduction bands of the nanotube are bent in order to adjust the Fermi level. Due to this band bending, the device has a very small conductivity for a small drain–source bias potential $V_{DS}$ (see Fig. 4(b)). The conductivity of the nanotube can be increased by several orders of magnitude by varying the gate voltage by a few volts above a threshold value. This is because the gate electric field reduces the bending of the bands of the nanotube. When it reaches the threshold value, the gate field aligns either the LUMO state or the HOMO state of the nanotube with the Fermi level of the drain or source electrodes, and a current starts flowing through the nanotube. Hence, depending on the gate potential, the transistor presents two states, OFF (low conductivity) and ON (high conductivity), as depicted in Fig. 4(b).

In today's FET devices, the insulating oxide layer between the gate and the nanotube is very thin. Thanks to the resulting high capacitive coupling to the nanotube, the gate signal can be amplified to a level such that the output voltage of a first transistor can control the input of a second one. This important technological improvement, plus the fact that both *p*-type, *n*-type, and ambipolar carbon nanotube FETs can be realized, makes it possible to integrate the nanotubes into elementary logical gates. Presently, state-of-the art carbon nanotubes transistors present performances comparable or even better than silicon metal-oxide-semiconductor field effect transistors (MOSFETs) (Avouris 2002).

### *3.3 Field Emission*

Due to their long aspect ratio (length to radius ratio), carbon nanotubes are suitable for electron field emission (de Heer *et al.* 1995). The basic theory of field emission is the Fowler–Nordheim equation that strictly applies to a semi-infinite free-electron medium, with a triangular barrier at the surface given by $V(z) = E_v - eFz$, where $z(>0)$ is the coordinate normal to the surface, $E_v$ is the vacuum energy, and $F$ is the electric field. Using the WKB approximation for the tunneling probability across the barrier, the expression of the current is (in A)

$$I = \frac{1.5610^{-6}A}{\phi}F^2 \exp\left(-\frac{6.8310^{9}\phi^{3/2}}{F}\right) \qquad (5)$$

where $A$ is the emission area in $m^2$, $F$ is in $V\,m^{-1}$, and $\phi$ is the work function in eV. For single-wall nanotubes, $\phi$ is typically 4.8 eV, slightly more than for multiwall nanotubes for which $\phi$ is 4.6 eV. Setting, for instance, $A = 5 \times 10^{-16}$ $m^2$ and $F = 5 \times 10^9$ $V\,m^{-1}$ leads to $I = 1.5$ nA.

Thanks to the long aspect ratio of a nanotube, the local electric field $F$ acting on the tip can be considerably larger than the applied field $V/D$, where $V$ is the applied voltage and $D$ is the distance between the nanotubes and the collecting anode. In Eqn. (5), $F = \beta V/D$ must be used, where the so-called amplification factor $\beta$ strongly depends on the type of nanotubes (single-wall, bundle of single-wall, or multiwall), on whether the tubes are open or not, and on

the morphology of the nanotube array. For an isolated nanotube, $\beta \sim 3 + L/R$; experimentally, $\beta$ is 200. In an array, there is a screening of the electric field when the density of nanotubes increases, which, in principle, reduces the amplification factor considerably compared to that of an isolated tube. Nevertheless, $\beta$ 2000 has been reported for some emitting nanotubes embedded in a film. Ideally, the distance between the nanotubes should be of the order of their length.

A great advantage of nanotubes for field-emission devices is that self-oriented arrays can be grown directly on a patterned electrode. Carbon nanotubes can work in normal vacuum conditions ($10^{-6}$ torr) under a reasonable threshold field: 2–10 $V\,\mu m^{-1}$ (applied field $V/D$). Closed multiwall nanotubes obtained by arc discharge have the best performances (Bonnard *et al.* 1999). A film of multiwall nanotubes can sustain a current density of 0.3 $mA\,cm^{-2}$ for a long duration. A single nanotube can emit a stable current of a few microamperes.

## 4. Summary

One of the most spectacular properties of single-wall carbon nanotubes is that they can be metallic or semiconducting, depending on their exact atomic structure. Metallic nanotubes are remarkable ballistic conductors, even at room temperature, while semiconducting single-wall nanotubes may become performant field effect transistors. Nanotubes are also good electron emitters. Possible applications of nanotubes, including nanoelectronic and optoelectronic devices, light sources, panel displays, etc., will exploit these properties, which are direct consequences of their atomic and electronic structures.

*See also*: Carbons: Bonding; Carbon Nanotubes; Electronic Structure of Fullerene-based Materials; Graphite Intercalation Compounds; Fullerites and Hard Carbons.

## Bibliography

Avouris Ph 2002 Carbon nanotube electronics. *Chem. Phys.* **281**, 429–45

Bachtold A, Fuhrer M S, Plyasunov S, Forero M, Anderson E H, Zettl A, McEuen P L 2000 Scanned probe microscopy of electronic transport in carbon nanotubes. *Phys. Rev. Lett.* **84**, 6082–5

Bockrath M, Cobden D H, Lu J, Rinzler A G, Smalley E E, Balents L, McEuen P L 1999 Luttinger-liquid behavior in carbon nanotubes. *Nature* **397**, 598–601

Bonnard J M, Salvetat J P, Stockli T, Forro L, Chatelain A 1999 Field emission from carbon nanotubes: perspectives for applications and clues to the emission mechanism. *Appl. Phys. A* **69**, 245–54

de Heer W A, Chatelain A, Ugarte D 1995 A carbon nanotube field-emission electron source. *Science* **270**, 1179–80

Ebbesen T W, Lezec H J, Hiura H, Bennett J W, Ghaemi H F, Thio T 1996 Electrical conductivity of individual carbon nanotubes. *Nature* **382**, 54–6

Fantini C, Jorio A, Souza M, Strano M S, Dresselhaus M S, Pimenta M A 2004 Optical transition energies for carbon nanotubes from resonant Raman spectroscopy: environment and temperature effects. *Phys. Rev. Lett.* **93**, 147406.1–4

Frank S, Poncharal Ph, Wang Z L, de Heer W A 1998 Carbon nanotube quantum resistors. *Science* **280**, 1744–6

Hamada N, Sawada S I, Oshiyama A 1992 New one-dimensional conductors: graphitic microtubules. *Phys. Rev. Lett.* **68**, 1579–81

Kane C L, Mele E J, Lee R S, Fischer J E, Petit P, Dai H, Thess A, Smalley R E, Verschueren A R M, Tans S J, Dekker C 1998 Temperature-dependent resistivity of single-wall carbon nanotubes. *Europhys. Lett.* **41**, 683–8

Landauer R 1970 Electrical resistance of disordered one-dimensional lattices. *Phil. Mag.* **21**, 863–7

Martel R, Schmidt T, Shea H R, Hertel T, Avouris Ph 1998 Single- and multi-wall carbon nanotube field-effect transistors. *Appl. Phys. Lett.* **73**, 2447–9

Popov V N (2004) Curvature effects on the structural, electronic and optical properties of isolated single-walled carbon nanotubes within a symmetry-adapted non-orthogonal tight-binding model. *New J. Phys.* **6**, 17.1–17

Rao A M, Richter E, Bandow S, Chase B, Eklund P C, Williams K A, Fang S, Subbaswamy K R, Menon M, Thess A, Smalley R E, Dresselhaus G, Dresselhaus M S 1997 Diameter-selective Raman scattering from vibrational modes in carbon nanotubes. *Science* **275**, 187–91

Tans S T, Verschueren A R M, Dekker C 1998 Room-temperature transistor based on a single carbon nanotube. *Nature* **393**, 49–52

Wallace P R 1947 The band theory of graphite. *Phys. Rev.* **71**, 622–34

Wildoer J W G, Venema L C, Rinzler A G, Smalley R E, Dekker C 1998 Electronic structure of atomically resolved carbon nanotubes. *Nature* **391**, 59–62

Ph. Lambin and V. N. Popov



Encyclopedia of Materials: Science and Technology
ISBN: 0-08-043152-6
pp. 1–7